Treatment of the $t\mu + D_2$ reaction by the methods of quantum reactive scattering

V. Zeman and E. A. G. Armour
School of Mathematical Sciences, University of Nottingham, Nottingham NG7 2RD, United Kingdom

R. T Pack
Theoretical Division (T-12, MS-B268), Los Alamos National Laboratory, Los Alamos, New Mexico 87545
(Received 13 July 1999; published 13 April 2000)

We have applied the methods of quantum reactive scattering to the key resonant reaction in the muon catalyzed fusion (MCF) cycle that leads to the formation of a $dt\mu$ muonic molecular ion, in which fusion takes place very rapidly. We have calculated reaction probabilities for the resonances that occur in $t\mu + D_2$ scattering for incident kinetic energies less than 0.6 eV and total angular momentum $J_{tot}=0$. To reduce the six-body problem to a three-body problem, the motions of the electrons were treated in the Born-Oppenheimer (BO) approximation while those of the muon were treated with a sophisticated adiabatic approximation. The resulting three-body potential energy surface (PES) was represented by a pairwise additive approximation. The $dt\mu$ part of the PES was scaled to allow it to exhibit the correct binding energy of the crucial $(J,v)=(1,1)$ state. Scattering calculations were carried out using a hyperspherical formulation, and the positions of the resonances were found to occur at energies of a few meV greater than if $dt\mu$ is assumed to be a point particle. A comparison of the resonances with the Breit-Wigner formula allowed us to calculate partial widths for back decay, $\Gamma_e^{J_{tot}}$. Once these are known for all significant J_{tot}, the rate of formation of $dt\mu$ can be determined. This rate, next to the sticking fraction, is the most important parameter in determining the rate of the entire MCF cycle. We have also carried out a calculation whereby the muon was treated in a BO formalism and have found significant differences in the final results, demonstrating the importance of treating the muon as accurately as possible. This work represents a successful *ab initio* calculation of this reaction.

PACS number(s): 34.50.−s, 36.10.Dr

I. INTRODUCTION

It has been known since about 1980 that a negatively charged muon in a deuterium-tritium mixture at room temperature can catalyze more than 100 nuclear fusion reactions. The muon (μ) first of all binds a deuteron (d) and a triton (t) to form the muonic molecular ion $dt\mu$, in which the two nuclei are so close together that fusion occurs very rapidly. Thereafter, the muon is usually released and is thus free to bring about further fusion reactions like a chemical catalyst. There exist a number of review articles on muon catalyzed fusion (MCF) in the literature [1–7].

One of the most important steps in the MCF cycle is the resonance mechanism, described by Vesman [8], that leads to $dt\mu$ formation. As is well known, this resonant reaction can take place because of a remarkable coincidence: $dt\mu$ has a weakly bound $(J,v)=(1,1)$ excited state with a nonrelativistic binding energy 0.66 eV, where J is the angular momentum of $dt\mu$ and $v=0,1,...$ denotes the vibrational states with angular momentum J in order of increasing energy.[1]

The key processes in this reaction are

$$\mathcal{T}+D_2 \underset{\text{back decay}}{\overset{\lambda_{dt\mu}}{\rightleftarrows}} [(dt\mu)_{11}dee] \underset{\text{Auger decay}}{\rightarrow} [(dt\mu)_{Jv}de]^+ + e, \tag{1.1}$$

where $D \equiv de$ and we have defined $\mathcal{T} \equiv t\mu$. To a good approximation, the $[(dt\mu)_{11}dee]$ complex can be regarded as a H_2-like molecule with one nucleus the particle d and the other the $dt\mu$ system in its (1,1) state. As a consequence of the very small binding energy of the (1,1) state, the energy of the reactants can equal the energy of excited rovibrational states of the intermediate complex in low-energy collisions. $dt\mu$ can also be formed in $\mathcal{T}+D_2$ collisions by nonresonant processes, but the rate of formation is much slower [9,5].

The resonant formation of the intermediate complex containing the $dt\mu$ molecule, with rate $\lambda_{dt\mu}$, is, next to the effective sticking fraction (the probability that in a given cycle a side reaction occurs in which the muon ends up bound to an α particle and is thus unable to catalyze any further fusion reactions), the most important parameter determining fusion efficiency [5]. Given that the muon lifetime is 2.2×10^{-6} sec, and that about 1000 fusion cycles should be catalyzed by a single muon for MCF to be considered a viable potential source of large-scale energy production, the cycle rate for the entire MCF reaction must be greater than a critical value of $\lambda_{crit}\approx 4\times10^8\,\text{sec}^{-1}$. The rate of formation of $dt\mu$ must also, therefore, be greater than this value. This rate is extremely energy (and therefore temperature) dependent due to the resonance mechanism of reaction (1.1). A detailed knowledge of how $\lambda_{dt\mu}$ behaves as a function of initial kinetic energy of the reactants in Eq. (1.1) is therefore crucial.

[1]Unfortunately, the practice of listing the vibrational quantum number last is deeply entrenched in the MCF literature. However, the standard practice in the spectroscopy, molecular physics, and chemistry communities is to use the notation (v,j), with $j=J$, to denote such states, where v and j are the vibrational and rotational quantum numbers, respectively. To minimize confusion, we will use here the MCF notation for $dt\mu$ but the standard notation for all other molecular species.

An experimental analysis of the dependence of $\lambda_{dt\mu}$ on the temperature [10], as well as on the density of the initial d-t mixture [11], was performed by Jones *et al.* in the 1980s. Their measured rates hovered around $\lambda_{\rm crit}$, thus highlighting the importance of an accurate knowledge of the behavior of $\lambda_{dt\mu}$. Another experimental investigation is currently in progress by Marshall and co-workers [12–14], while Nagamine *et al.* [15] expect to begin experiments shortly.

A. Previous calculations

Previous treatments [16–24] of reaction (1.1) have been based on the Breit-Wigner formula for the resonant total cross section $\sigma_a(E)$ for the Auger process. Men'shikov and Faifman [18], for example, take this to be of the form

$$\sigma_a(E)=\frac{\pi}{k^2}\sum_{J_{\rm tot}=0}^{\infty}(2J_{\rm tot}+1)\frac{\Gamma_e^{J_{\rm tot}}\Gamma_a^{J_{\rm tot}}}{(E-E_r)^2+\frac{1}{4}(\Gamma_e^{J_{\rm tot}}+\Gamma_a^{J_{\rm tot}})^2}, \tag{1.2}$$

where E is the energy of the relative motion of $\mathcal{T}$ and D_2, $\mathbf{k}$ is the associated wave vector, and E_r is the energy of the resonant state r under consideration, relative to the energy of $\mathcal{T}$ and D_2 at infinite separation. The partial widths are defined as follows: $\Gamma_e^{J_{\rm tot}}$ is the back decay partial width for total angular momentum $J_{\rm tot}$ and $\Gamma_a^{J_{\rm tot}}$ is the corresponding partial width for the Auger decay process. Equation (1.2) neglects any target angular momentum and any spin angular momentum on the $\mathcal{T}$, but these can easily be taken into account.

Using the relation that [16,18,25–28]

$$\Gamma_e^{J_{\rm tot}}\ll\Gamma_a^{J_{\rm tot}}\ll E_r, \tag{1.3}$$

an approximate expression can be obtained for $\sigma_a(E)$ of the form [16,18]

$$\sigma_a(E)\approx\frac{2\pi^2}{k^2}\Gamma_e\delta(E-E_r), \tag{1.4}$$

where

$$\Gamma_e=\sum_{J_{\rm tot}=0}^{\infty}(2J_{\rm tot}+1)\Gamma_e^{J_{\rm tot}}. \tag{1.5}$$

Thus, in this approximation, the key parameter in determining $\sigma_a(E)$ is Γ_e, which is determined from a knowledge of the partial widths $\{\Gamma_e^{J_{\rm tot}}\}_{J_{\rm tot}=0}^{\infty}$ for the *back decay* process. In deriving Eq. (1.4), the resonances are treated as being of zero width. The effect of resonance broadening is taken into account by Petrov and Petrov [22,23].

The resonant rate of formation of $dt\mu$, at a temperature T, is given by

$$\lambda_{dt\mu}(T)=n_{D_2}\int v_c(E)\sigma_a(E)f(E,T)dE, \tag{1.6}$$

where n_{D_2} is the density of the D_2 molecules, $v_c(E)$ is the collision velocity of $\mathcal{T}$ relative to D_2, and $f(E,T)$ is a distribution function, which is usually assumed to be a Maxwell distribution, due to the thermal spread of $v_c(E)$. The two most recent calculations [23,24] both yield $\lambda_{dt\mu}(T)$ values that vary around $\lambda_{\rm crit}$, once again emphasizing the necessity for an accurate determination of $\lambda_{dt\mu}$ as a function of temperature (and therefore kinetic energy). It is our aim to perform ab initio calculations of $\lambda_{dt\mu}$. As a start toward this goal we have performed calculations for total angular momentum $J_{\rm tot}=0$ using the methods of quantum reactive scattering.

B. The challenge

The treatments based on the Breit-Wigner formula are, in part, phenomenological. The challenge is to carry out a detailed quantum mechanical treatment of the reaction (1.1). We have shown [29] how a Breit-Wigner type formula for $\sigma_a(E)$ arises from a detailed close-coupling treatment of the reaction (1.1). However, the approach we used would be very complicated to apply numerically. An alternative approach is to adopt the methods of quantum reactive scattering that have already been applied to chemical reactions [30–32]. We gave an account of how this might be done in a previous publication [33].

Chemical reactions such as

$$H+D_2\leftrightarrow HD+D \tag{1.7}$$

have been extensively studied using quantum mechanical methods. Reaction (1.1) is similar to reaction (1.7) in that they both involve collisions between D_2 and an atom containing particles of unit positive and negative charge. However, comparison of reactions (1.1) and (1.7) shows that reaction (1.1) has special features not present in reaction (1.7), notably the Auger decay process which leads to the loss of an electron. Equation (1.7) corresponds quite closely to the much slower side reaction

$$\mathcal{T}+D_2\leftrightarrow\mathcal{T}D+D, \tag{1.8}$$

where $\mathcal{T}D=[(dt\mu)_{J_v}e]$. This reaction proceeds through the same resonances as reaction (1.1),

$$\mathcal{T}+D_2\leftrightarrow[(dt\mu)_{11}dee]\rightarrow\mathcal{T}D+D. \tag{1.9}$$

In this case the resonant complex decays forward into the muonic molecule $[(dt\mu)_{J_v}e]$ and a D atom or backward into $\mathcal{T}+D_2$. Reaction (1.9) can be treated using methods that have been applied to reaction (1.7). In this paper, we present results obtained by applying the method that Pack and Parker [30] have developed for rearrangement scattering reactions of this type. An important question we face is how to obtain information relevant to reaction (1.1) from our treatment of reaction (1.9).

There is no easy way of including the Auger decay channel directly in our present treatment. We assume that, for a given partial wave, the resonant cross section for decay into the products on the right-hand side (RHS) of Eq. (1.9) is given by the Breit-Wigner formula

$$\sigma_n^{J_{\rm tot}}(E)=\frac{\pi}{k^2}(2J_{\rm tot}+1)\frac{\Gamma_e^{J_{\rm tot}}\Gamma_n^{J_{\rm tot}}}{(E-E_r)^2+\frac{1}{4}(\Gamma_e^{J_{\rm tot}}+\Gamma_n^{J_{\rm tot}}+\Gamma_a^{J_{\rm tot}})^2}, \tag{1.10}$$

where $\Gamma_n^{J_{\rm tot}}$ is the partial width for the decay of the complex into the products on the RHS of Eq. (1.9). As we are not including the Auger decay process, $\Gamma_a^{J_{\rm tot}}=0$ in our calculations. As pointed out by Men'shikov and Faifman [18], the coupling between the resonant channels is small as the lifetime of the resonant complex is much longer than the time the complex takes to complete a vibration. Thus, the various decay processes operate essentially independently, and we should be able to obtain accurate values for $\Gamma_n^{J_{\rm tot}}$ and $\Gamma_e^{J_{\rm tot}}$ by fitting our results for resonant total cross sections to formula (1.10) with $\Gamma_a^{J_{\rm tot}}$ set to zero [33]. As pointed out earlier, quite accurate values of $\sigma_a(E)$ can be obtained from a knowledge of $\Gamma_e^{J_{\rm tot}}$. If required, values of $\Gamma_a^{J_{\rm tot}}$ can be obtained from a number of calculations [25–28].

II. THE INTERACTION POTENTIAL

The system here $[dt\mu dee]$ consists of six particles, each of which has a unit positive or negative charge. In a nonrelativistic treatment at this stage, the total potential energy is the sum of all the Coulombic attractions and repulsions between the particles. However, an accurate treatment of the problem at the six-body level is not presently possible. To simplify the problem, we note that for this low-energy scattering problem the electrons move much faster than the nuclei, and we use the familiar Born-Oppenheimer (BO) approximation to solve for the electronic motions with the nuclei held fixed, average over the motions of the electrons, and obtain an effective potential for the nuclear motions. Furthermore, although the muon is intermediate in mass between the electrons and the nuclei, it stays so close to the nuclei that it moves even faster than the electrons, and we can also average over its motions with the nuclei held fixed. However, its mass is not negligible compared to the nuclear masses, and we treat it with a sophisticated adiabatic approximation discussed in Sec. II B to account for that.

Use of these two approximations has the effect of excluding the Auger decay already discussed, but it should allow all other accessible processes to be treated quite accurately. It reduces the six-body problem to a three-body problem where the bodies are the muonic and electronic atoms denoted in Eq. (1.8), and they move on the resulting effective potential energy surface (PES). This greatly reduces the complexity of the problem.

If the electronic-muonic problem just described were solved accurately, it would require expensive computations in which the motions of the muon and the electrons were correlated and would yield a complicated three-body PES. We hope to do that in future calculations. However, for the purposes of this reactive scattering calculation on this system, we note that the $\mathcal{T}$ atom is very small (about 200 times smaller than a D atom), and it has only a tiny polarizability. As a result, it has an appreciable interaction with only one of the D atoms at a time, even if it is inside the electronic charge cloud of the D_2 molecule. Because of this, we use a pairwise additive approximation to the PES; i.e.,

$$V=V_{\rm DD'}+V_{\mathcal{T}\rm D}+V_{\mathcal{T}\rm D'}, \tag{2.1}$$

where $V_{\rm DD'}$, for example, represents the interaction between the two D atoms. Each of these diatomic potentials depends only on the distance between the two atoms. This pairwise additive approximation includes some effects of the finite size of muonic atoms and molecules but omits others, and these will be discussed further in Sec. II C.

The interaction $V_{\rm DD'}$ is the familiar BO potential for the hydrogen molecule. It has been calculated accurately by Kołos and Wolniewicz [34], and we use their results in the present calculations.

$V_{\mathcal{T}\rm D}$ and $V_{\mathcal{T}\rm D'}$ represent the adiabatic interaction between the $\mathcal{T}$ and the D atoms. This attraction cannot be calculated accurately enough using the BO approximation, as the ratio of the mass of the muon to the mass of the nuclei is too large. In this case, the mass of the muon $m_\mu=206.8m_e$ and therefore $m_\mu=0.056m_d$. Thus, in the following subsection we start with the BO approximation and discuss ways in which more accurate results can be obtained.

A. The Born-Oppenheimer and standard adiabatic approximations

The total Hamiltonian for the internal motion of the $dt\mu$ system is

$$\hat{H}=-\frac{1}{2m_{dt}}\nabla_{\mathbf{R}}^2-\frac{1}{2m_{\mu(dt)}}\nabla_{\mathbf{r}}^2+\frac{1}{R}-\frac{1}{r_{d\mu}}-\frac{1}{r_{t\mu}}, \tag{2.2}$$

where $\mathbf{R}$ represents the internuclear vector pointing from the lighter nucleus (d) to the heavier (t), and $\mathbf{r}$ is the position vector of the muon, relative to the center of mass of the nuclei. The reduced masses are defined as

$$m_{dt}=\frac{m_d m_t}{m_d+m_t}, \quad m_{\mu(dt)}=\frac{m_\mu(m_d+m_t)}{m_\mu+m_d+m_t}. \tag{2.3}$$

In the BO approximation the effective d-t potential is obtained by fixing the nuclei and calculating the energy of the resulting system, $V_{\rm BO}(R)$, as a function of the internuclear distance R. In this approximation, the BO wave functions for $dt\mu$ are written in separated form:

$$\Psi_{\rm BO}^i(\mathbf{r},\mathbf{R})=F^i(\mathbf{R})\,\phi_{\rm BO}^i(\mathbf{r};R), \tag{2.4}$$

where i represents a particular solution and the muonic wave functions $\phi_{\rm BO}^i(\mathbf{r};R)$ depend only parametrically on R. The $V_{\rm BO}(R)$ of interest is the lowest ($i=0$) eigenvalue of the Schrödinger equation,

$$\hat{H}_{\rm BO}\phi_{\rm BO}^0(\mathbf{r};R)=V_{\rm BO}(R)\,\phi_{\rm BO}^0(\mathbf{r};R), \tag{2.5}$$

where

$$\hat{H}_{\mathrm{BO}} = -\frac{1}{2m_\mu}\nabla_{\mathbf{r}}^2 + \frac{1}{R} - \frac{1}{r_{d\mu}} - \frac{1}{r_{t\mu}}. \tag{2.6}$$

The Schrödinger equation (2.5) can be solved exactly if both sides are expressed in terms of prolate spheroidal coordinates, as this equation is separable in these coordinates [35]. For the method of evaluation as applied to H_2^+, see, for example, Bates *et al.* [36] and Wind [37]. Details of the solution to a three-particle system in general are given, for example, by Hunter and Pritchard [38].

The standard adiabatic (SA) approximation is the lowest-order correction to the BO approximation. Whereas in the BO approximation all coupling between the muonic and nuclear motion is omitted, in the SA approximation the effect of the coupling term involving $\nabla_{\mathbf{R}}^2 \phi_{\mathrm{BO}}^0(\mathbf{r};R)$ is included in the potential to first order using perturbation theory. This can be regarded as including in the potential the effect on the nuclear motion of the averaged motion of the muon in its ground state. Thus,

$$V_{\mathrm{SA}}(R) = V_{\mathrm{BO}}(R) + \langle \phi_{\mathrm{BO}}^0(\mathbf{r};R) | \hat{H}' | \phi_{\mathrm{BO}}^0(\mathbf{r};R) \rangle_{\mathbf{r}}, \tag{2.7}$$

where the perturbation correction to the BO Hamiltonian is

$$\hat{H}' = \hat{H} - \hat{H}_{\mathrm{BO}} = -\frac{1}{2m_{dt}}\nabla_{\mathbf{R}}^2 - \frac{1}{2(m_d+m_t)}\nabla_{\mathbf{r}}^2. \tag{2.8}$$

The BO and SA approximations are particularly unsuitable for accurate calculations of asymmetric diatomic molecules. This is because the BO wave functions are symmetric with respect to the two nuclei. For the $dt\mu$ molecule, for example, this results in an incorrect dissociation at large R to an equal mixture of $d\mu + t$ and $t\mu + d$. Since $t\mu$ has a lower ground state energy than $d\mu$, the correct dissociation products should be $t\mu + d$. Pack [39,40] has shown how to solve this problem within an adiabatic formalism; prior to this it was thought that computationally expensive nonadiabatic methods were necessary.

For further details concerning the SA approximation and its limitations, see, for example, the review by Kołos [41].

B. The improved adiabatic and higher-order approximations

The improved adiabatic (IA) approximation was developed by Struensee *et al.* [42]. It is a modification of the ''best adiabatic'' (BA) method [40,43], which was the first to yield the correct dissociation energy at large R for asymmetric molecules without the use of a nonadiabatic formalism. The IA method also yields correct dissociation energies, but has been found to be more reliable than the BA at smaller R.

In the IA approximation the effect of the angular motion of the nuclei is included in the potential. Instead of adding a perturbation correction to the BO potential, we start with a potential that is calculated by treating the nuclei as a rigid rotor. The Hamiltonian in Eq. (2.2) is separated into

$$\hat{H} = \hat{H}_{\mathrm{IA}}^0 + \hat{H}_{\mathrm{IA}}', \tag{2.9}$$

where

$$\hat{H}_{\mathrm{IA}}^0 = \hat{H}_{\mathrm{BO}} - \frac{1}{2(m_d+m_t)}\nabla_{\mathbf{r}}^2 + \frac{\hat{L}_R^2}{2m_{dt}R^2} \tag{2.10}$$

and

$$\hat{H}_{\mathrm{IA}}' = -\frac{1}{2m_{dt}}\left(\frac{\partial^2}{\partial R^2} + \frac{2}{R}\frac{\partial}{\partial R}\right). \tag{2.11}$$

$\hat{L}_{\mathbf{R}}$ is the operator for the relative angular motion of the nuclei. The wave function is a sum of terms which are seperated into components in a similar way as in Eq. (2.4), except here the nuclear component is a function of only the internuclear distance and the muonic component is a function of the remaining five coordinates, and depends only parametrically on the internuclear distance,

$$\Psi_{\mathrm{IA}}(\mathbf{r},\mathbf{R}) = \sum_i \chi^i(R)\phi_{\mathrm{IA}}^i(\mathbf{r},\hat{\mathbf{R}};R). \tag{2.12}$$

The ground state ($i=0$) zeroth order potential is then evaluated by solving

$$\hat{H}_{\mathrm{IA}}^0 \phi_{\mathrm{IA}}^0(\mathbf{r},\hat{\mathbf{R}};R) = U_{\mathrm{IA}}(R)\phi_{\mathrm{IA}}^0(\mathbf{r},\hat{\mathbf{R}};R). \tag{2.13}$$

The IA potential $V_{\mathrm{IA}}(R)$ of Struensee *et al.* [42] is obtained by adding the lowest-order perturbation term to $U_{\mathrm{IA}}(R)$ due to the action of $\hat{H}_{\mathrm{IA}}'$ on $\phi_{\mathrm{IA}}^0(\mathbf{r},\hat{\mathbf{R}};R)$. Since, for a real IA wave function that is normalized at all R, it can easily be shown that

$$\left\langle \phi_{\mathrm{IA}}^0(\mathbf{r},\hat{\mathbf{R}};R) \left| \frac{2}{R}\frac{\partial}{\partial R} \right| \phi_{\mathrm{IA}}^0(\mathbf{r},\hat{\mathbf{R}};R) \right\rangle_{\mathbf{r},\hat{\mathbf{R}}} = 0, \tag{2.14}$$

where the integration is over the variables that precede the semicolon, it follows that the IA potential of Struensee *et al.* is given by

$$V_{\mathrm{IA}}(R) = U_{\mathrm{IA}}(R) - \frac{1}{2m_{dt}}\left\langle \phi_{\mathrm{IA}}^0(\mathbf{r},\hat{\mathbf{R}};R) \left| \frac{\partial^2}{\partial R^2} \right| \phi_{\mathrm{IA}}^0(\mathbf{r};\hat{\mathbf{R}};R) \right\rangle_{\mathbf{r},\hat{R}}. \tag{2.15}$$

As can be seen, for example, from the variational calculation of the energy of the (1, 1) state of $dt\mu$ by Bhatia *et al.* [26], to a very good approximation the angular momentum of $dt\mu$ is located on the nuclei. Thus in the IA approximation the muon can be taken with high accuracy to be in a σ state with zero angular momentum about the internuclear axis. In this case the summation in the IA wave function of Eq. (2.12) collapses to only one term and, as pointed out by Struensee *et al.* [42], the IA potential for nonzero angular momentum can be obtained by simply adding the centrifugal term $J(J+1)/(2m_{dt}R^2)$ to the IA potential for $J=0$.

The use of muonic wave functions $\phi_{\mathrm{IA}}^i(\mathbf{r},\hat{\mathbf{R}};R)$, which are functions of the internuclear unit vector $\hat{\mathbf{R}}$, and the presence of the term involving $\hat{L}_{\mathbf{R}}^2$ in the associated Hamiltonian $\hat{H}_{\mathrm{IA}}^0$ ensure that the muon remains close to the triton at large

R. $V_{IA}(R)$ therefore has (virtually) the correct energy at large R, corresponding to the binding energy of the $t\mu$ atom. $V_{SA}(R)$, on the other hand, exhibits an incorrect asymptotic energy corresponding to the average of the binding energies of $t\mu$ and $d\mu$. The improved adiabatic behavior of $V_{IA}(R)$ comes about because the IA approximation incorporates all of the terms from the SA approximation, but also some terms that would normally be considered nonadiabatic in the standard formalism [44].

As is shown in Sec. IV A, the IA potential gives considerably more accurate values for the binding energies of the five bound states of $dt\mu$ than do the BO or SA potentials. It breaks the symmetry, so that for the lowest state the muonic wave function shifts over onto the triton as R gets large. However, because the second term in Eq. (2.15) enters perturbationally rather than variationally, this shift occurs too rapidly, and the second term in the equation gets too large and produces a small unphysical barrier at around $8a_\mu$. That this barrier is unphysical was shown by Cohen and Struensee [44] who did two-state nonadiabatic coupled channel calculations on $dt\mu$ using an IA internal basis. The two states they included use the potential energy curves that at large R correspond to the two channels $t\mu+d$ and $d\mu+t$. No sign of the barrier appears in their scattering results because off diagonal radial coupling terms cause the effects of the barrier to cancel. Unfortunately, the values of Cohen and Struensee [44] for the two terms of Eq. (2.15) are no longer available [45] but an approximation to the first term was obtained as follows. Cohen and Struensee [44] did perform an adiabatic to diabatic transformation on their equations, and the resulting 2×2 diabatic potential matrix was still available [45]. This was diagonalized and the resulting derivative coupling neglected. Its lower root gave a potential which is smooth and which dissociates properly to the $t\mu+d$ limit. We have used this potential here and will refer to it as having been calculated in the IA+ approximation.

To convert the $dt\mu$ potential into an effective $D\mathcal{T}$ potential, the effect of electron screening has been added perturbatively. Cohen and Struensee [44] have calculated the electronic component in a BO formalism, and we have used their results in our calculation.

Relativistic and QED effects are not formally included in any of the potentials that we have used. As is discussed further in Sec. IV A, the shift in binding energies caused by these and other nonadiabatic effects is incorporated into our calculations by scaling the $dt\mu$ potential such that it exhibits the correct binding energy of 0.5966 eV. This assumes that the $dt\mu$ molecule remains in its lowest $F=0$ hyperfine state throughout the entire reaction, where F is the spin of the $\mathcal{T}$ atom (i.e., $\hat{\mathbf{F}}=\hat{\mathbf{S}}_t+\hat{\mathbf{S}}_\mu$). This is a valid assumption due to the smallness of relativistic effects and the large size of the hyperfine splitting [46].

C. Finite-size effects and resonance positions

In Eq. (2.1) we have taken the PES to be pairwise additive. This includes some of the effects due to the finite size of the $\mathcal{T}D$ and omits others. It includes the effect due to the finite size of the equilibrium bond length of this molecule. However, in the current potential the electrons always see a particle of unit charge at the position of the deuteron for all d-t distances. This is correct at large and at very small d-t distances. However, at intermediate d-t distances, a more accurate calculation would allow the electrons to see the shift of the muon density and thus to see partial charges on both the d and the t that change with d-t distance.

An approximation neglecting all finite-size effects has been previously used [47,48] to calculate the energies of the various bound states of $[(dt\mu)_{11}dee]$. In those calculations the entire $dt\mu$ molecule was treated as a point particle so that the six-body complex was treated equivalently to a diatomic molecule. Using their calculations one can estimate the positions of the resonances based on the conservation of energy:

$$E[\mathcal{T}]+E[D_2]_{v_i j_i}+E^{\mathrm{kin}}_{\nu K}=E[Xdee]_{\nu K}+E[dt\mu]_{11}, \tag{2.16}$$

where $X\equiv dt\mu$, $m_X=m_d+m_t+m_\mu$, (v_i,j_i) are the rovibrational quantum numbers of the initial D_2 molecule, and (ν, K) are the rovibrational quantum numbers corresponding to bound states of the fictitious diatomic molecule where $dt\mu$ is treated as a point particle. In this equation, $E^{\mathrm{kin}}_{\nu K}$ corresponds to the relative kinetic energy between $\mathcal{T}$ and D_2 that gives rise to a resonance corresponding to a particular (ν, K). However, since we have included some finite-size effects in our calculations, the kinetic energies that give rise to resonances according to Eq. (2.16) will not exactly match the positions of our resonances.

Furthermore, conservation of angular momentum requires that

$$\hat{\mathbf{J}}_{\mathrm{tot}}=\hat{\mathbf{J}}+\hat{\mathbf{K}}. \tag{2.17}$$

Since the angular momentum of $dt\mu$ is $J=1$, and in our calculation we have only considered $J_{\mathrm{tot}}=0$, then we must have $K=1$. We therefore cannot yet account for resonance broadening effects due to multiple values of K (for nonzero J_{tot}).

Harston *et al.* [52] have performed perturbation calculations intended to yield a value for the finite-size corrections to the energy of $[(dt\mu)_{11}dee]$. They have obtained corrections up to first order in accuracy, but have concluded that a precise estimate would require the evaluation of higher-order terms. A prediction for the finite-size corrections for the six-body complex, which is expected to be of the order of several meV, is therefore presently unavailable. However, Harston *et al.* [53] have obtained a value of 0.5 meV for the finite-size correction to the $(dt\mu)_{11}e$ molecule, resulting in a binding energy of 0.5961 eV. We have scaled our $D\mathcal{T}$ potentials so that they give this value for the binding energy of the (1,1) state.

Finally, we have neglected corrections to the $F=0$ hyperfine energy levels of the $\mathcal{T}$ atom that are due to the presence of the other particles. These corrections constitute a shift of less than 1 meV [46].

III. THE SCATTERING CALCULATION IN THE APH FORMALISM

In this section we briefly review the scattering theory in the APH (adiabatically adjusting, principal axes hyperspherical) formalism for $J_{\rm tot}=0$ and outline details particular to the present calculation. Further details concerning the APH method for nonzero $J_{\rm tot}$ are given by Pack and Parker [30]. A sample of some of the subsequent calculations using this method, with emphasis on its practical application, is given in Refs. [49–51].

A. The APH coordinates

The choice of coordinates that are appropriate for the geometry of the system under consideration is essential to obtaining accurately converged results in a minimum amount of time when performing scattering calculations that require a large amount of computation. In the case of reactive scattering where the initial reactants (e.g., $\mathcal{T}+D_2$) are different from the final products (e.g., $D+D\mathcal{T}$), it is convenient to use a coordinate system that transforms smoothly from one arrangement to the other. Hyperspherical coordinates have been found to satisfy this condition, and a number of different types have been used for atom-diatom reactive scattering calculations (see, for example, Refs. [30–32]). The coordinates that we have used are the *adiabatically adjusting, principal axes hyperspherical* (APH) coordinates [30]. In what follows, we review how the APH coordinates are related to other well-known but less sophisticated coordinates.

Let us denote the atoms, for example, in reaction (1.7), by *A*, *B*, and *C*, with *A* the atom in the entrance channel. There are three possible sets of *Jacobi coordinates* $\{\mathbf{R}_\tau,\mathbf{r}_\tau\}$ $(\tau=A,B,C)$, depending on which scattering channel is under consideration. Thus, for example, $\mathbf{R}_A$ is the position vector of atom *A* with respect to the center of mass of atoms *B* and *C* as origin, and $\mathbf{r}_A$ is the position vector of atom *C* relative to atom *B*.

The *mass-scaled Jacobi coordinates* are defined as [30]

$$\mathbf{S}_\tau=d_\tau\mathbf{R}_\tau,\quad \mathbf{s}_\tau=\mathbf{r}_\tau/d_\tau, \tag{3.1}$$

where

$$d_\tau=\left[\frac{m_\tau}{\bar{m}}\left(1-\frac{m_\tau}{M}\right)\right]^{1/2},\quad \bar{m}=\left[\frac{m_Am_Bm_C}{M}\right]^{1/2}, \tag{3.2}$$

and $M=m_A+m_B+m_C$ is the total mass of the system. The resulting kinetic energy operator is symmetric in that the same reduced mass factor is applied to both of its components, i.e.,

$$\hat{T}=-\frac{1}{2\bar{m}}(\nabla^2_{\mathbf{s}_\tau}+\nabla^2_{\mathbf{S}_\tau}). \tag{3.3}$$

This property proves to be advantageous when transforming to other coordinate systems.

The APH coordinates are obtained by performing an orthogonal transformation,

$$\begin{bmatrix}\mathbf{Q}\\ \mathbf{q}\end{bmatrix}=\mathbf{T}(\chi_\tau)\begin{bmatrix}\mathbf{S}_\tau\\ \mathbf{s}_\tau\end{bmatrix}, \tag{3.4}$$

where $\mathbf{T}(\chi_\tau)$ is the proper, orthogonal 6×6 matrix,

$$\mathbf{T}(\chi_\tau)=\begin{bmatrix}\cos\chi_\tau\mathbf{I} & \sin\chi_\tau\mathbf{I}\\ -\sin\chi_\tau\mathbf{I} & \cos\chi_\tau\mathbf{I}\end{bmatrix}, \tag{3.5}$$

and $\mathbf{I}$ is the 3×3 unit matrix. The kinematic angle χ_τ is a continuous variable, with τ denoting its origin. As $\chi_\tau\to0$, $\mathbf{Q}$ and $\mathbf{q}$ become $\mathbf{S}_\tau$ and $\mathbf{s}_\tau$. This angle is converted into an APH coordinate, χ_i, where i denotes the initial scattering arrangement, by choosing it to take on a value that maximizes $Q=|\mathbf{Q}|$. This is possible as χ_i is a function of S_τ, s_τ, and Θ_τ. Such a choice results in $\mathbf{Q}$ and $\mathbf{q}$ being in the directions of the instantaneous principal axes of inertia of the system in the plane of the atoms, with associated moments of inertia $\bar{m}q^2$ and $\bar{m}Q^2$, respectively. Also, as atom τ becomes infinitely far from the other two atoms,

$$\lim_{\substack{S_\tau\to\infty\\ (s_\tau\text{finite})}}\mathbf{Q}=\pm\mathbf{S}_\tau. \tag{3.6}$$

This supplies the desired link between the three channels.

The APH internal coordinates (in the plane of the atoms) are defined by $\{\rho,\theta,\chi_i\}$, where

$$\theta=\frac{\pi}{2}-2\tan^{-1}(q/Q), \tag{3.7}$$

and the hyperradius is defined by

$$\rho=(Q^2+q^2)^{1/2}=(S_\tau^2+s_\tau^2)^{1/2}. \tag{3.8}$$

Note that as $\mathbf{T}(\chi_\tau)$ is orthogonal, ρ is invariant under the transformation (3.4). These coordinates are very suitable for describing rearrangement processes since they (i) adjust adiabatically to follow any atom that leaves the other two, (ii) treat all arrangements equivalently, and (iii) make possible a smooth transition between channels. They are particularly suitable for our purposes as they give a dynamical description of the resonant complex $[(dt\mu)_{11}dee]$ that occurs in both reaction (1.9) and reaction (1.1).

In practice it is often convenient to transform to a simpler set of coordinates outside the exchange region, when one atom is far away from the other two. In our calculation we transform to *Delves coordinates*. For a given arrangement τ, these are defined by the hyperradius ρ, as in Eq. (3.8), the hyperangle

$$\vartheta_\tau=\tan^{-1}(s_\tau/S_\tau), \tag{3.9}$$

and Θ_τ, the angle between $\mathbf{s}_\tau$ and $\mathbf{S}_\tau$.

B. The scattering calculation

The total Hamiltonian in APH coordinates, for $J_{\rm tot}=0$, takes the following form:

$$\hat{H}=-\frac{\hbar^2}{2\bar{m}\rho^5}\frac{\partial}{\partial\rho}\rho^5\frac{\partial}{\partial\rho}-\frac{\hbar^2}{2\bar{m}\rho^2}\times\left(\frac{4}{\sin 2\theta}\frac{\partial}{\partial\theta}\sin 2\theta\frac{\partial}{\partial\theta}+\frac{1}{\sin^2\theta}\frac{\partial^2}{\partial\chi_i^2}\right)+V(\rho,\theta,\chi_i). \tag{3.10}$$

Here $V(\rho,\theta,\chi_i)$ is the potential energy surface. It depends only on the three internal coordinates. In our calculations V is the pairwise additive potential of Eq. (2.1).

In the calculations the ρ range is divided into a number of intervals or sectors. On the ξth sector, the overall $J_{\rm tot}=0$ wave function Ψ^n of the system is expanded in a basis set of ''sector adiabatic'' or ''diabatic-by-sectors'' ''surface functions'' $\Phi_t(\theta,\chi_i,\rho_\xi)$, which are determined at the center of the sector, ρ_ξ:

$$\Psi^n=\frac{\sqrt{2}}{\pi}\rho^{-5/2}\sum_t\ \psi_t^n(\rho)\Phi_t(\theta,\chi_i;\rho_\xi), \tag{3.11}$$

where $\psi_t^n(\rho)$ is regular at $\rho=0$ and $n=1,...,N$ denotes the particular solution under consideration. The inclusion of Wigner D functions of the APH (external) Euler angles in Eq. (3.11) would be necessary if $J_{\rm tot}$ were nonzero. For $J_{\rm tot}=0$ only even parity ($p=0$) solutions exist.

Use of this wave function gives the coupled channel scattering equations as [30]

$$\left(\frac{\partial^2}{\partial\rho^2}+\frac{2\bar{m}E}{\hbar^2}\right)\psi_t^n(\rho)=\frac{2\bar{m}}{\hbar^2}\sum_{t'}\ \langle\Phi_t(\theta,\chi_i;\rho)|\hat{H}_i|\Phi_{t'}(\theta,\chi_i;\rho)\rangle\psi_{t'}^n(\rho), \tag{3.12}$$

where

$$\hat{H}_i=-\frac{\hbar^2}{2\bar{m}\rho^2}\left(\frac{4}{\sin 2\theta}\frac{\partial}{\partial\theta}\sin 2\theta\frac{\partial}{\partial\theta}+\frac{1}{\sin^2\theta}\frac{\partial^2}{\partial\chi_i^2}\right)+\frac{15\hbar^2}{8\bar{m}\rho^2}+V(\rho,\theta,\chi_i), \tag{3.13}$$

and E is the total energy of the system. Equations (3.12) are solved for ρ values in a finite number of intervals or sectors, ranging from $\rho_{\rm min}$ to $\rho_{\rm max}$. $\rho_{\rm min}$ is chosen such that all surface function eigenvalues are strongly repulsive, while $\rho_{\rm max}$ is well outside the exchange region. The scattering parameters are determined by carrying out an orthogonal transformation at $\rho_{\rm max}$ from the APH wave functions to laboratory fixed Delves wave functions, writing the asymptotic Jacobi coordinate wave functions in terms of Delves coordinates, and matching them to obtain the reactance or **K** matrix.

The surface functions $\Phi_t(\theta,\chi_i,\rho_\xi)$ are independent of ρ in each sector as they are determined at ρ_ξ, the center of the sector. These functions are obtained by solving a two-dimensional Schrödinger equation on the surface of the hypersphere,

$$\hat{H}_i\Phi_t(\theta,\chi_i;\rho_\xi)=\mathcal{E}_t(\rho_\xi)\Phi_t(\theta,\chi_i;\rho_\xi). \tag{3.14}$$

The surface function eigenvalues $\mathcal{E}_t(\rho_\xi)$ represent effective potentials for the ρ motion to the extent that this motion is slow enough that the θ and χ_i motions can adjust adiabatically. In the asymptotic region of the infinite ρ the off-diagonal matrix elements in Eq. (3.12) become zero and $\mathcal{E}_t(\rho_\xi)$ become equivalent to the diatomic bound state energies.

In our calculations, for $\rho<0.92$, the surface functions were obtained by using a finite element method (FEM). These methods are ideal at small ρ where the surface functions are delocalized over much of the surface of the hypersphere. However, as ρ is increased and the arrangement channels become more localized in small regions of the surface, FEMs require the use of very fine grids and become inefficient to use. Eventually, due to computational limitations, it becomes impossible to obtain accurately converged surface functions. We used as fine a grid as we found was possible, with over 500 intervals in θ and over 2000 intervals in χ_i. A second method which is often used at small ρ in quantum reactive scattering calculations is the discrete variable representation (DVR) method. This method is usually more efficient than FEMs at larger values of ρ, but in cases like the present calculation where one diatomic molecule (e.g., D$\mathcal{T}$) has a much shorter bond length than another (e.g., D_2), FEMs prove to be more efficient [50].

For $\rho>0.92$ an analytic basis method (ABM) [50] was used. This method uses basis functions that are analytic, simple harmonic functions of an anharmonic variable, allowing for the inclusion of anharmonicity. The basis functions are centered in the arrangement channels and therefore result in a very compact representation at large ρ. While this ABM method works well for most reactions involving diatomic molecules where the potential as a function of ϑ_τ is nearly harmonic, we experienced difficulties in obtaining converged results for the arrangement involving D$\mathcal{T}$, which is an extremely anharmonic molecule. We solved this by modifying the basis functions to better allow for the case of anharmonic molecules. The details of this are given in the Appendix. In our calculation we used basis functions with rovibrational quantum numbers up to $(v,j)=(14,22)$ for D_2 and (30,3) for D$\mathcal{T}$.

In our calculations we used 515 different hyperradial sectors by varying ρ logarithmically from $0.66a_0$ to $10a_0$. The surface functions corresponding to the lowest 50 eigenvalues $\mathcal{E}_t(\rho)$ were calculated, and 50 close-coupled equations were then propagated using the log derivative method [54]. Two separate calculations were performed using two different PESs, corresponding to treating the $dt\mu$ potential in the BO and IA+ formalisms as outlined in Sec. II. Resonances were located by performing calculations around the expected resonance energies, given by Eq. (2.16) for $E_{v1}^{\rm kin}<0.6$ eV. The resonances were then mapped out by performing calculations with energy increments of about 0.1 meV, and interpolation was used in between these mesh points.

The calculations were performed on a Sun Ultra 1 computer, which needed about 1 week of CPU time to calculate

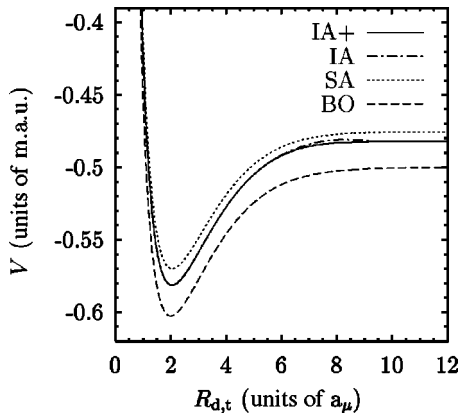

FIG. 1. Potential energies of $dt\mu$ as a function of the *internuclear* distance, calculated using various approximations. Distances and energies are in muonic atomic units where $a_\mu=(m_e/m_\mu)a_0$ and 1 m.a.u.$=(m_\mu/m_e)$ a.u.

the surface functions and about 1 hour of CPU time per scattering energy to propagate the close-coupling equations.

IV. RESULTS

A. The $dt\mu$ potential

As outlined in Sec. II, the muon to nuclei mass ratio is too large for the applicability of the BO approximation. The most accurate calculation to date of a $dt\mu$ potential which is a function of only the internuclear distance R has been performed in the IA approximation by Struensee *et al.* [55]. There have also been a large number of variational calculations performed which have resulted in much more accurate values of the $dt\mu$ binding energies (see, for example, the review articles by Froelich [5] and Ponomarev [3] for a comparison of these).

We have calculated the $dt\mu$ potential and the binding energies of the various (J,v) states in the BO and SA formalisms as outlined in Sec. II A. We have also used the IA potential calculated Struensee *et al.* [55] as well as the IA+ potential, as outlined in Sec. II B, using the calculations of Cohen and Struensee [44]. These potentials, as a function of the internuclear distance, are shown in Fig. 1. Only the IA and IA+ potentials dissociate at large R to the correct asymptotic limit corresponding to the binding energy of $t\mu$. The main difference between these two potentials is the presence of an unphysical barrier in the IA potential.

The SA approximation yields a potential energy function $V_{\mathrm{SA}}(R)$ that represents an upper bound for the exact potential energy at any R [41]. However, this does not mean that the binding energy of any particular state is necessarily a lower bound to the exact value. This is because the binding energy is defined to be the difference between the dissociation energy at infinite R and the energy of a bound state. The binding energies of the bound states are compared with the nonrelativistic ''exact values'' in Table I. Although the total energies of the bound states are more accurately predicted by the SA approximation than by the BO, the overcompensation of the dissociation energy in the SA approximation results in binding energies that are less accurate (more tightly bound) than in the BO.

TABLE I. Binding energies of $dt\mu$ (J,v) states calculated using potentials obtained in various approximations as outlined in Sec. II, and compared to the exact nonrelativistic values. All energies are in units of eV.

(J,v)	Exact nonrelativistic	BO	SA	IA	IA+
(1,1)	0.66	8.4	15.7	~ -2	0.97
(0,1)	34.83	43.7	53.3	31.2	33.71
(2,0)	101.42	106.6	123.3	99.9	100.54
(1,0)	232.47	239.4	253.9	230.3	230.75
(0,0)	319.14	329.2	340.9	317.2	317.74

The IA potential, however, gives binding energies that are about a factor of 10 more accurate, but, due to the unphysical barrier, the crucial $(J,v)=(1,1)$ state is calculated to be slightly unbound. However, the IA+ potential yields a (1,1) binding energy value of 0.97 eV. The binding energies of all five states are most accurately calculated using the IA+ potential.

The potential $V_{D\mathcal{T}}$, as required for the PES of Eq. (2.1), is interpreted as being a function of the interatomic distance (i.e., the distance from the center of mass of D to the center of mass of $\mathcal{T}$); the binding energies of the various $dt\mu$ potentials considered in Table I have assumed the radial coordinate to be the internuclear distance. This approximation is almost equivalent to the replacement of m_{dt} in Eq. (2.15) with $m_{D\mathcal{T}}$. The resulting binding energies for the IA+ potential are shown in Table II. The effects of electronic screening were taken into account [44] through a BO formalism and added to the $dt\mu$ potential to convert it into a D$\mathcal{T}$ potential. This IA+ potential was then scaled in such a way as to yield a precise D$\mathcal{T}$(1,1) binding energy, including relativistic and QED effects, of 0.5961 eV. This value incorporates a 0.5 meV shift [53] of the $dt\mu(1,1)$ binding energy when taking into account electronic screening. The resulting binding energies of all five states are shown in the last column of Table II.

The potentials were scaled by first shifting the curves shown in Fig. 1 so that their asymptotic energies are zero, and then stretching them in the vertical and/or horizontal

TABLE II. Binding energies of the original IA+$dt\mu$ potential, after replacing m_{dt} with $m_{D\mathcal{T}}$, and after scaling to yield the exact relativistic value for the (1,1) state. All energies are in units of eV.

(J,v)	Exact relativistic	Original IA+	$m_{dt}\rightarrow m_{D\mathcal{T}}$	After scaling
(1,1)	0.60	0.97	2.12	0.60
(0,1)	34.77	33.71	33.45	31.95
(2,0)	101.42[a]	100.54	103.93	96.31
(1,0)	232.58	230.75	233.25	224.02
(0,0)	319.41	317.74	319.30	309.53

[a]Relativistic and QED corrections are unknown for this state.

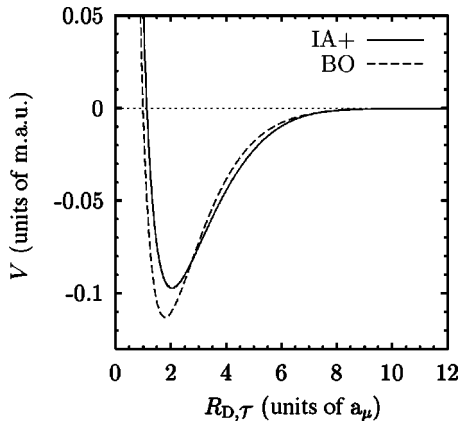

FIG. 2. Potential energies of $dt\mu$ as a function of the *interatomic* distance, in the BO and IA+ approximations after scaling to yield the exact value for the binding energy of the (1,1) state. Both potentials have been shifted so that their asymptotic values approach zero. Distances and energies are in muonic atomic units where $a_\mu=(m_e/m_\mu)a_0$ and 1 a.m.u.$=(m_\mu/m_e)$ a.u.

directions such that they yield the correct binding energy for the (1,1) state, using the pairwise additive potential. For the IA+ curve, this was done by multiplying in the vertical direction by a factor of 0.977, i.e., $V_{\mathrm{IA}+}^{\mathrm{scaled}}(R)=0.977V_{\mathrm{IA}+}^{\mathrm{unscaled}}(R)$. The BO curve was scaled according to $V_{\mathrm{BO}}^{\mathrm{scaled}}(R)=1.101V_{\mathrm{BO}}^{\mathrm{unscaled}}(0.899R)$. A comparison of the resulting scaled potentials is shown in Fig. 2. Since we have used the pairwise additive potential for calculating the binding energies in this scaling procedure, the radial distance no longer corresponds to the internuclear distance, but the interatomic distance.

B. The potential energy surface and surface functions

In Fig. 3 we show the 50 lowest surface function eigenvalues $\mathcal{E}_t(\rho)$ for the IA+ calculation, obtained by solving the two-dimensional Schrödinger equation of Eq. (3.14). In this figure zero energy is defined as the sum of the binding energies of the initial reactants in their ground states, i.e., $E[\mathcal{T}]+E[D_2]_{00}$. In the asymptotic region of large ρ, the bottom four curves correspond to the four lowest states of D$\mathcal{T}$. The remaining network of curves correspond, in the asymptotic region, to D$\mathcal{T}$(1,1) and the various D_2 states.

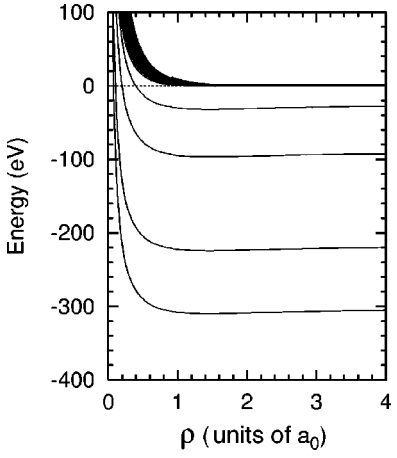

FIG. 3. The lowest 50 surface function eigenvalues $\mathcal{E}_t(\rho)$ for the IA+ calculation. The bottom four curves correspond asymptotically to the lowest four bound states of D$\mathcal{T}$. Zero energy is defined as the ground state of the initial reactants.

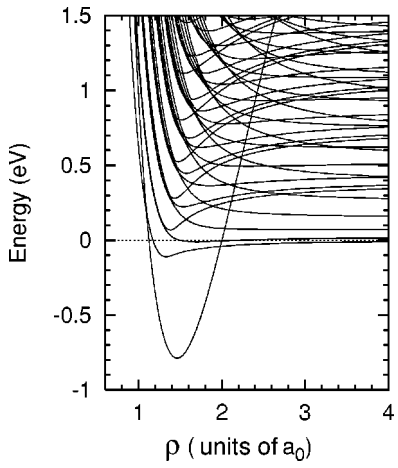

FIG. 4. As in Fig. 3, magnified to show the intersection of the curve that asymptotically corresponds to D$\mathcal{T}$(1,1) with the curves that asymptotically correspond to the various D_2 states. The D$\mathcal{T}$(1,1) curve is the one that exhibits the deepest well in this figure.

At $\rho=0.92$ there is a slight discontinuity in each of the curves due to the switchover from the FEM to the ABM. This discontinuity is more evident for higher states, which are not as important as the lower ones. Also, apart from the four lowest curves, which are not very important with regard to the intermediate resonant complex, the eigenvalues at $\rho=0.92$ are all well above the classically forbidden boundary for the low scattering energies considered here.

Figure 4 is a magnified version of Fig. 3, which clearly shows the eigenvalues of the state that corresponds to D$\mathcal{T}$(1,1) in the asymptotic region as it intersects the various $D_2(v,j)$ states. The former curve is the one that exhibits the deepest well. The reaction proceeds by initially starting on one of the D_2 states at large ρ. As the $\mathcal{T}$ atom approaches D_2, ρ decreases until it attains a certain critical value at which there no longer exists a potential barrier between the two $\mathcal{T}+D_2$ and D$\mathcal{T}$+D arrangements, allowing exchange to take place. For ρ less than this value, the intermediate resonant complex $[(dt\mu)_{11}dee]$, which corresponds to the curve with the deepest well, is very likely to form. The curve corresponding to the resonant complex is clearly classically forbidden in the asymptotic region. In the muon catalyzed fusion reaction (1.1), after the system has oscillated in this potential well for a while, the complex is then most likely to undergo irreversible decay by an Auger process. For our calculation corresponding to reaction (1.9), the most probable event is for the complex to transfer to one of the curves corresponding to a D_2 state in the asymptotic region. However, it is also possible that the resonant complex will decay to one of the four bottom curves that asymptotically correspond to D$\mathcal{T}$.

A three-dimensional plot of the PES calculated using the IA+D$\mathcal{T}$ potential, at $\rho=1.7a_0$, is shown in Fig. 5. Here we

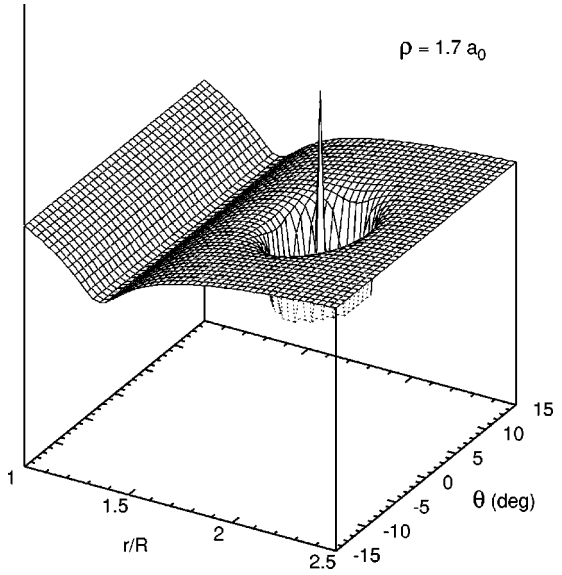

FIG. 5. The current PES of the $[dt\mu dee]$ system plotted in terms of the Delves coordinates for the $D_2+\mathcal{T}$ arrangement, at $\rho=1.7a_0$, using the IA+ approximation for the $dt\mu$ potential. The energy has been plotted using a logarithmic scale, and the bottom of the D$\mathcal{T}$ well has been artificially truncated.

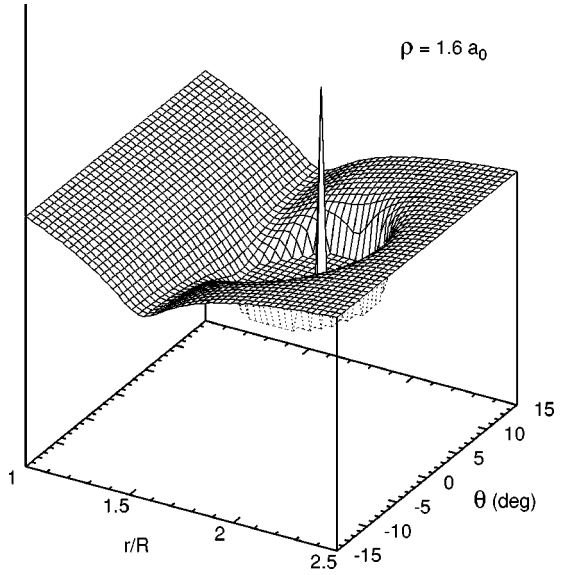

FIG. 6. As in Fig. 5 for $\rho=1.6a_0$.

have used coordinates similar to Delves, corresponding to the $D_2+\mathcal{T}$ arrangement. In these coordinates, the $r/R=0$ line corresponds to the overlapping of the two D atoms, while the $(r/R=2,\Theta=0)$ point corresponds to a $\mathcal{T}$ atom overlapping with one of the D atoms. For $\rho=1.7a_0$ there are two separate potential ''wells'': the line at about $r/R=1.35$ corresponds to the well around the D_2 molecule, while the circular feature around the peak at $(r/R=2,\Theta=0)$ corresponds to the well around D$\mathcal{T}$. Initially, as the $\mathcal{T}$ atom approaches the D_2 molecule and ρ is decreasing, the linear well associated with D_2 moves closer to the circular well associated with D$\mathcal{T}$. At a critical value of ρ, the two wells touch each other so that there no longer exists a potential barrier between the two arrangements. This occurs at around $\rho=1.6a_0$, as shown in Fig. 6. The removal of the potential barrier that classically forbids a rearrangement reaction from proceeding first occurs at $\Theta=0$, corresponding to a linear configuration of the three atoms. As ρ is decreased further the two wells continue to merge together, as demonstrated by Fig. 7 where $\rho=1.5a_0$. For ρ smaller than 1.5, the well moves into the repulsive region of the D_2 potential.

C. Reaction probabilities: resonances

The surface functions calculated from Eq. (3.14) were used to solve the close-coupling Eqs. (3.12), from which the reactance matrix and reaction probabilities were calculated. For rearrangement reactions where the initial $D_2(v_ij_i)$ molecule reacts with a $\mathcal{T}$ atom to yield a D atom and a $\mathcal{T}D(v_fj_f)$ molecule, the reaction probability is related to the cross section by

$$\sigma_n^{J_{\rm tot}}(v_ij_i\rightarrow v_fj_f)=\frac{\pi}{k_i^2}(2J_{\rm tot}+1)P^R_{v_ij_i}(v_fj_f). \qquad (4.1)$$

The total reaction probability or reactivity for a particular initial channel is obtained by summing over the reaction probabilities of all possible final rovibrational states, i.e.,

$$P^R_{v_ij_i}=\sum_{v_fj_f}P^R_{v_ij_i}(v_fj_f). \qquad (4.2)$$

In our case there are only four final rovibrational states that can form owing to energy considerations, corresponding to the four lowest D$\mathcal{T}$ states. In Fig. 8 we present the total reactivities, for the IA+ calculation, for initial D_2 rovibrational states of (v_i,j_i) equal to (0,0), (0,2), and (1, 0). These represent the ground, first rotationally excited, and first vibrationally excited states (nuclear symmetry allows only transitions in D_2 that result in even changes of j). The energy E on the horizontal axes of this figure corresponds to the

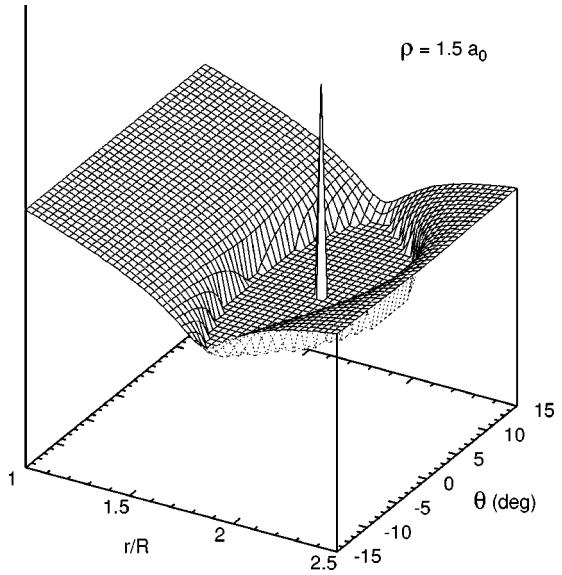

FIG. 7. As in Fig. 5 for $\rho=1.5a_0$.

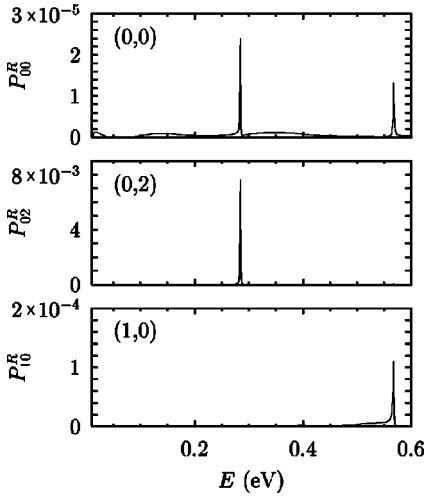

FIG. 8. Total reactivities of the IA+ calculation, with the initial D_2 molecule in its ground (0, 0), first rotationally excited (0, 2), and first vibrationally excited (1, 0) states. The energy is with respect to the D_2 ground state.

initial kinetic energy relative to the ground (0,0) state of D_2. The kinetic energy corresponding to the scattering of $\mathcal{T}$ from the $D_2(0,2)$ state, for example, would then be equal to $E-E[D_2]_{02}+E[D_2]_{00}$. This figure demonstrates the dominance of the resonant behavior of the $\mathcal{T}+D_2$ reaction over the nonresonant behavior. The resonances shown correspond to $\nu=3$ and $\nu=4$ in Eq. (2.16). For the (0,2) state, the $\nu=4$ resonance is much weaker than the $\nu=3$ resonance and therefore cannot be seen in this figure. For the (1,0) state, the threshold energy is such that only $\nu\geqslant4$ resonances are possible.

A magnified version of this figure around the energies corresponding to the $\nu=3$ resonance is shown in Fig. 9, and around the energies corresponding to $\nu=4$ in Fig. 10. Also shown in these figures are the total reactivities corresponding to the BO calculation. There are significant differences in both position and magnitudes of the resonances, depending on whether the IA+ or BO approximations are used for the $dt\mu$ potential. The positions of the resonances are compared in Table III with those that are obtained in the approximation where $dt\mu$ is treated as a point particle. The kinetic energy resonance positions in this approximation, $E^{\rm kin}_{\nu1}$, are calculated from Eq. (2.16). For $\nu=3$, the resonances in the IA+ approximation are found to occur at energies of about 4 meV greater than $E^{\rm kin}_{31}$, while in the BO approximation they occur at about 1 meV greater. The position of the $\nu=4$ resonance is about 5 meV greater than $E^{\rm kin}_{41}$, in the IA+ approximation, and about 2 meV greater in the BO approximation. Since our calculation does include some finite-size effects, differences of about this magnitude were expected. The center of the $\nu=2$ resonance is calculated to occur just slightly below threshold, but since we have considered only the case of $J_{\rm tot}=0$, resonance broadening due to excitation of higher rotational levels of the intermediate complex has not been included in our calculations. The rotational energy of $[Xdee]_{\nu K}$, for a given vibrational quantum number ν, is about $2.5K(K+1)$ meV.

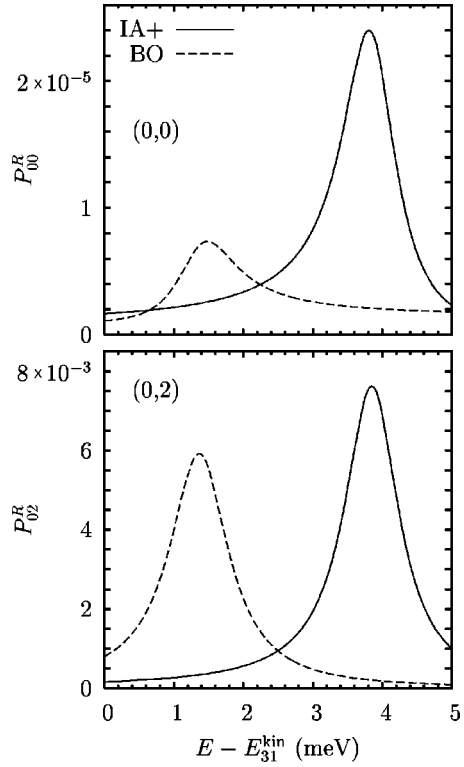

FIG. 9. Magnification of Fig. 8 around the $\nu=3$ resonance, also showing the BO calculation. From Table III, $E^{kin}_{31}=281.0$ meV.

The partial widths for reactive scattering, Γ^0_n, and the partial widths for backscattering, Γ^0_e, were calculated by fitting the total reactivities to the Breit-Wigner formula (1.10), with Γ^0_a set equal to zero,

$$P^R_{v_ij_i}(E)=\frac{\Gamma^0_e\Gamma^0_n}{(E-E_r)^2+\frac{1}{4}(\Gamma^0_e+\Gamma^0_n)^2}. \tag{4.3}$$

This was done by using the method of least squares to obtain optimum values for the variables E_r, Γ^0_e, and Γ^0_n for energies where $P^R_{v_ij_i}(E)$ was calculated to be greater than half of its maximum value $P^R_{v_ij_i}(E_r)$. Although Eq. (4.3) is symmetric with respect to the two partial widths, the values of the two widths were found to differ by several orders of magnitude. Our results for nonreactive scattering indicate that the probability for elastic backscattering is much greater than that for any other process, and we were thus able to assign Γ^0_e to the larger of the two partial widths in Eq. (4.3), and Γ^0_n to the smaller. Although our calculations for Γ^0_e do not include contributions from the inelastic backscattering process, since elastic backscattering was found to strongly dominate, this omission should be virtually negligible.

Use of the hyperradius in all configurations makes the derivation of the Breit-Wigner formula for the resonant cross sections similar to that of Mott and Massey [56]. Our resonances were found to fit this formula quite closely. We found that the position of the resonances remained almost the same if coupling between channels was omitted, but the height of the resonant cross sections altered significantly. This shows

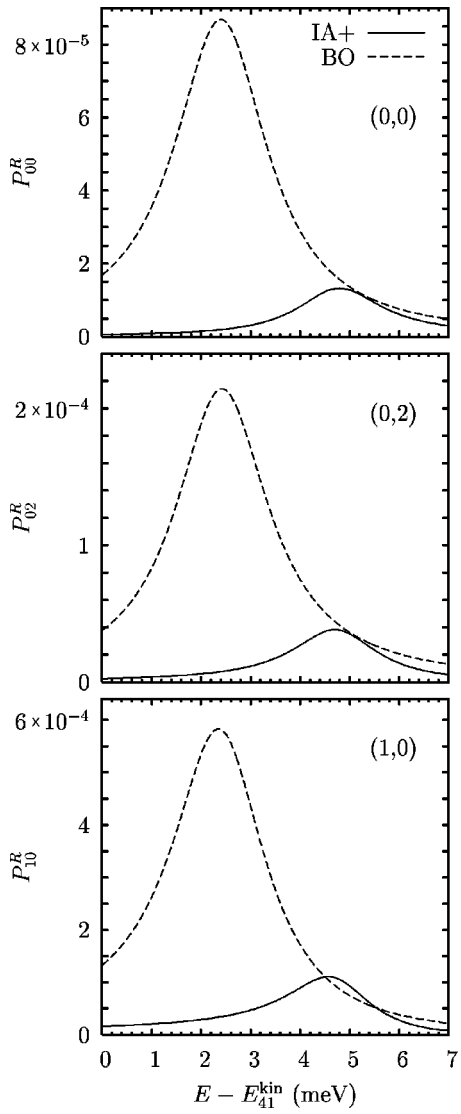

FIG. 10. Magnification of Fig. 8 around the $\nu=4$ resonance, also showing the BO calculation. From Table III, E_{41}^{kin} $=562.0$ meV.

that the wave functions used to evaluate directly the partial widths in the Breit-Wigner formula must take this coupling into account, if accurate results are to be obtained.

In Tables IV and V we show Γ_n^0 and Γ_e^0, for the resonances shown in Figs. 9 and 10. There are significant differences between the IA+ and BO calculations for Γ_n^0, while Γ_e^0 appears to be more stable. For the $\nu=3$ resonance the partial width for back decay is about 1 meV, while for the $\nu=4$ resonance it is on the order of 2 meV. As shown in Sec. I A, the rate of formation of $dt\mu$, and therefore the theoretical limit on the rate of the entire MCF cycle, is essentially dependent upon Γ_e.

TABLE III. Positions of the energy resonances with respect to the ground-state energy of D_2. $E_{\nu1}^{\rm kin}$ corresponds to the positions of the resonances for $J_{\rm tot}=0$, and therefore $K=1$, in the approximation where all finite-size effects are omitted and $dt\mu$ is treated as a point particle, in accordance with Eq. (2.16). All energies are in units of eV.

ν	$E_{\nu1}^{\rm kin}$	E(IA+)	E(BO)
2	-0.0101	<0	<0
3	0.2810	0.285	0.282
4	0.5620	0.567	0.564

TABLE IV. Back decay partial widths of the $\nu=3$ reactive scattering resonances, Γ_e^0, and the corresponding reactive partial widths, Γ_n^0, for $J_{\rm tot}=0$. All energies are in units of eV.

(v_i,j_i)	Γ_e^0(IA+)	Γ_n^0(IA+)	Γ_e^0(BO)	Γ_n^0(BO)
(0,0)	1.0×10^{-3}	6.0×10^{-9}	1.4×10^{-3}	2.5×10^{-9}
(0,2)	1.0×10^{-3}	1.8×10^{-6}	1.0×10^{-3}	1.5×10^{-6}

V. CONCLUSIONS

We have made a successful application of the APH method of quantum reactive scattering by Pack and Parker [30] to the treatment of the key $\mathcal{T}+D_2$ reaction in the muon catalyzed fusion cycle, for $J_{\rm tot}=0$. We have used an adiabatic potential that takes into account, as far as possible, important corrections to the Born-Oppenheimer approximation due to the fact that the muon is much more massive than the electron. Remaining inaccuracies are substantially reduced by scaling. We have demonstrated that the BO approximation leads to results that are significantly different from those obtained from a sophisticated adiabatic treatment of the muon, although the partial widths for backscattering are somewhat more stable.

In our calculations the resonances in the rearrangement channel occur at energies a few meV greater than where they are predicted to occur if finite-size effects are omitted and $dt\mu$ is considered to be a point particle. It is clear that the rearrangement reaction essentially proceeds only through the resonances. This is a vivid illustration of the mechanism for muonic molecule formation first suggested by Vesman [8] to explain the temperature dependence of the cross section for $dd\mu$ formation.

It has not been possible at this stage to include directly the Auger channel that leads to the most rapid formation of $dt\mu$ in a state with $J=0$, in which fusion takes place within about 10^{-12} sec[3]. We have instead considered the reaction (1.9), which proceeds through the same resonances of the intermediate complex $[(dt\mu)_{11}dee]$ as in the muon catalyzed fusion reaction (1.1), and have demonstrated how the rate of forma-

TABLE V. Back decay partial widths of the $\nu=4$ reactive scattering resonances, Γ_e^0, and the corresponding reactive partial widths, Γ_n^0, for $J_{\rm tot}=0$. All energies are in units of eV.

(v_i,j_i)	Γ_e^0(IA+)	Γ_n^0(IA+)	Γ_e^0(BO)	Γ_n^0(BO)
(0,0)	2.1×10^{-3}	7.0×10^{-9}	2.3×10^{-3}	5.0×10^{-8}
(0,2)	2.1×10^{-3}	2.0×10^{-8}	2.3×10^{-3}	1.2×10^{-7}
(1,0)	2.2×10^{-3}	6.2×10^{-8}	2.3×10^{-3}	3.3×10^{-7}

tion of $dt\mu$, which imposes the theoretical limit to the efficiency of the entire MCF cycle, can be obtained from such a treatment. This essentially involves the calculation of the back decay partial widths, $\Gamma_e^{J_{\rm tot}}$. We have calculated these widths, for $J_{\rm tot}=0$, to be about 1 meV for the $\nu=3$ resonance of the intermediate complex and about 2 meV for $\nu=4$.

The next step in these calculations should therefore be to incorporate states with $J_{\rm tot}>0$. This would allow us to calculate $\Gamma_e^{J_{\rm tot}}$ for all $J_{\rm tot}$, and therefore $\lambda_{dt\mu}(T)$. A future improvement to our method would be to include the Auger channel directly into the calculation, rather than relying on the Breit-Wigner formula. Also, improving the PES used would include all finite-size effects.

ACKNOWLEDGMENTS

We are very grateful to J. S. Cohen for his invaluable assistance with the IA+ potential and for his continuing interest in this work. We would also like to thank G. A. Parker for his assistance with the APH codes, and B. Kendrick, I. Shimamura, and J. Wallenius for helpful and stimulating discussions. We also thank S. B. Padkjaer and E. A. Butcher for preliminary calculations on this reaction which helped to guide the present work. Finally, we wish to thank EPSRC (U.K.) for their support of our research through Grant No. GR/L29170.

APPENDIX: IMPROVEMENT TO THE ABM BASIS FUNCTIONS

The ABM method was developed by Parker and Pack [50]. In determining the surface functions in a given sector as functions of the APH angular coordinates θ and χ_f in the τ_fth arrangement channel, it is convenient to transform to Delves angular coordinates ϑ_f and Θ_f for the channel under consideration. These coordinates are described at the end of Sec. III A.

This is an efficient way of obtaining surface functions that satisfy the requirement of being centered in arrangement channel τ_f. Θ_f is the internal rotational angle of the three-body system. Thus the dependence of a given basis function on this variable can be taken into account by including, as a factor, an associated Legendre function, expressed in terms of $\cos\Theta_f$.

The variable ϑ_f describes what is basically a vibrational motion. The dependence of the basis functions on this variable can be taken into account by using simple harmonic functions expressed in terms of an anharmonic variable z_f. This variable is a function of ϑ_f chosen so as to match the desired equilibrium position, fundamental frequency, and anharmonicity for the basis functions.

Full details of the method are given in the paper by Parker and Pack [50]. However, for molecules such as D$\mathcal{T}$, for which the potential as a function of ϑ_f is extremely anharmonic, the convergence of the surface functions as the number of basis functions is increased is very slow. In this appendix we make a change in the form of z_f to increase the rate of convergence in this case.

As can be seen from Eqs. (17)–(19) of Ref. [48], the ϑ_f dependent part of the basis functions in the original ABM method was chosen to be

$$\frac{\Upsilon_f(\vartheta_f;\rho)}{\sin 2\vartheta_f}\approx\frac{1}{B_f(\vartheta_f)}\phi_{\nu_f}(z_f), \tag{A1}$$

where ϕ is a simple harmonic oscillator function of z_f,

$$\phi_{\nu_f}(z_f)=\frac{1}{[\pi^{1/2}2^{\nu_f}(\nu_f!)]^{1/2}}H_{\nu_f}(z_f)e^{-z_f^2/2}, \tag{A2}$$

and the anharmonic variable takes the form

$$z_f=a_f\tan\vartheta_f-\frac{b_f}{\tan\vartheta_f}+c_f. \tag{A3}$$

Equation (A3), corresponding to Eq. (19) of Ref. [48], is replaced with

$$z_f=a_f\tan^n\vartheta_f-\frac{b_f}{\tan^n\vartheta_f}+c_f, \tag{A4}$$

where $n=1$ corresponds to z_f of Eq. (A3). As n is decreased the basis functions should behave more like Morse functions at large ρ, as shown by Schwenke [57]. In order for the new primitive basis to retain orthonormality, the normalization factor of Eq. (23) in Ref. [48] is replaced with

$$B_f(\vartheta_f)=\left(\frac{\sin^{n+3}(2\vartheta_f)}{n2^{n-1}(a_f\sin^{2n}\vartheta_f+b_f\cos^{2n}\vartheta_f)}\right)^{1/2}, \tag{A5}$$

and the parameters of Eqs. (A11)–(A13) of Ref. [48] are replaced with

$$a_f=\frac{\cos^{n+1}\vartheta_{M_f}}{6n^2\sin^{n-1}\vartheta_{M_f}}\left(3(n-\sin^2\vartheta_{M_f}+\cos^2\vartheta_{M_f})g_2^{1/2}+\frac{g_3}{g_2^{1/2}}\sin\vartheta_{M_f}\cos\vartheta_{M_f}\right), \tag{A6}$$

$$b_f=\frac{\sin^{n+1}\vartheta_{M_f}}{6n^2\cos^{n-1}\vartheta_{M_f}}\left(3(n+\sin^2\vartheta_{M_f}-\cos^2\vartheta_{M_f})g_2^{1/2}-\frac{g_3}{g_2^{1/2}}\sin\vartheta_{M_f}\cos\vartheta_{M_f}\right), \tag{A7}$$

$$c_f=b_f\cot^n\vartheta_{M_f}-a_f\tan^n\vartheta_{M_f}. \tag{A8}$$

In our calculations we have found that a value of $n=0.6$ allows for convergence of the D$\mathcal{T}$(1,1) state to within 0.1 meV using basis states with maximum vibration number $v=30$, instead of up to $v=70$ which is required for $n=1$.

[1] A. K. Bhatia and R. J. Drachman, Comments At. Mol. Phys. **22**, 281 (1989).
[2] W. H. Breunlich, P. Kammel, J. S. Cohen, and M. Leon, Annu. Rev. Nucl. Part. Sci. **39**, 311 (1989).
[3] L. I. Ponomarev, Contemp. Phys. **31**, 219 (1990).
[4] H. E. Rafelski, D. Harley, G. R. Shin, and J. Rafelski, J. Phys. B **24**, 1469 (1991).
[5] P. Froelich, Adv. Phys. **41**, 405 (1992).
[6] E. A. G. Armour, M. R. Harston, and M. P. Faifman, in *The Physics of Electronic and Atomic Collisions: XVII International Conference*, edited by T. Andersen, B. Fastrup, F. Folkmann, H. Knudson, and N. Andersen, AIP Conf. Proc. No. 295 (AIP, New York, 1993), p. 478.
[7] J. S. Cohen, in *Review of Fundamental Processes and Applications of Atoms and Ions*, edited by C. D. Lin (World Scientific, Singapore, 1993), Chap. 2.
[8] E. A. Vesman, Zh. Eksp. Teor. Fiz. Pis'ma Red. **5**, 113 (1967) [JETP Lett. **5**, 91 (1967)].
[9] M. P. Faifman, Muon Catal. Fusion **4**, 341 (1989).
[10] S. E. Jones, A. N. Anderson, A. J. Caffrey, J. B. Walter, K. D. Watts, J. N. Bradbury, P. A. M. Gram, M. Leon, H. R. Maltrud, and M. A. Paciotti, Phys. Rev. Lett. **51**, 1757 (1983).
[11] S. E. Jones, A. N. Anderson, A. J. Caffrey, C. DeW. Van Siclen, K. D. Watts, J. N. Bradbury, J. S. Cohen, P. A. M. Gram, M. Leon, H. R. Maltrud, and M. A. Paciotti, Phys. Rev. Lett. **56**, 588 (1986).
[12] G. M. Marshall *et al.*, Hyperfine Interact. **118**, 89 (1999).
[13] M. C. Fujiwara (unpublished).
[14] T. A. Porcelli (unpublished).
[15] K. Nagamine, T. Matsuzaki, K. Ishida, S. N. Nakamura, and N. Kawamura, Hyperfine Interact. **119**, 273 (1999).
[16] A. M. Lane, Phys. Lett. **98A**, 337 (1983).
[17] L. I. Men'shikov, Yad. Fiz. **42**, 1184 (1985) [Sov. J. Nucl. Phys. **42**, 750 (1985)].
[18] L. I. Men'shikov and M. P. Faifman, Yad. Fiz. **43**, 650 (1986) [Sov. J. Nucl. Phys. **43**, 414 (1986)].
[19] A. M. Lane, J. Phys. B **20**, 2911 (1987).
[20] A. M. Lane, J. Phys. B **21**, 2159 (1988).
[21] M. P. Faifman, L. I. Men'shikov, and T. A. Strizh, Muon Catal. Fusion **4**, 1 (1989).
[22] V. Yu. Petrov and Yu. V. Petrov, Muon Catal. Fusion **4**, 73 (1989).
[23] Yu. V. Petrov and V. Yu. Petrov, Phys. Lett. B **378**, 1 (1996).
[24] M. P. Faifman, T. A. Strizh, E. A. G. Armour, and M. R. Harston, Hyperfine Interact. **101**, 179 (1996).
[25] S. I. Vinitsky, L. I. Ponomarev, and M. P. Faifman, Zh. Eksp. Teor. Fiz. **82**, 985 (1982) [Sov. Phys. JETP **55**, 578 (1982)].
[26] A. K. Bhatia, R. J. Drachman, and L. Chatterjee, Phys. Rev. A **38**, 3400 (1988).
[27] A. Scrinzi and K. Szalewicz, Phys. Rev. A **39**, 2855 (1989).
[28] E. A. G. Armour, D. M. Lewis, and S. Hara, Phys. Rev. A **46**, 6888 (1992).
[29] E. A. G. Armour, Phys. Rev. A **52**, 1982 (1995).
[30] R. T Pack and G. A. Parker, J. Chem. Phys. **87**, 3888 (1987); **90**, 3511 (1989).
[31] D. E. Manolopoulos and D. C. Clary, Annu. Rep. Prog. Chem., Sect. C: Phys. Chem. **86**, 95 (1989).
[32] D. E. Manolopoulos, M. D'Mello, and R. E. Wyatt, J. Chem. Phys. **93**, 403 (1990).
[33] E. A. G. Armour, J. Chem. Soc., Faraday Trans. **93**, 1011 (1997).
[34] W. Kolos and L. Wolniewicz, J. Mol. Spectrosc. **54**, 303 (1975).
[35] L. P. Eisenhart, Phys. Rev. **74**, 87 (1948).
[36] D. R. Bates, K. Ledsham, and A. L. Stewart, Philos. Trans. R. Soc. London, Ser. A **246**, 215 (1953).
[37] H. Wind, J. Chem. Phys. **43**, 2956 (1965).
[38] G. Hunter and H. O. Pritchard, J. Chem. Phys. **46**, 2146 (1967).
[39] R. T Pack and J. O. Hirschfelder, J. Chem. Phys. **49**, 4009 (1968).
[40] R. T Pack, Phys. Rev. A **32**, 2022 (1985).
[41] W. Kołos, Adv. Quantum Chem. **5**, 99 (1970).
[42] M. C. Struensee, J. S. Cohen, and R. T Pack, Phys. Rev. A **34**, 3605 (1986).
[43] R. T Pack and J. O. Hirschfelder, J. Chem. Phys. **52**, 521 (1970).
[44] J. S. Cohen and M. C. Struensee, Phys. Rev. A **43**, 3460 (1991).
[45] J. S. Cohen (private communication).
[46] D. Bakalov, K. Bakalova, V. Korobov, H. J. Monkhorst, and I. Shimamura, Phys. Rev. A **57**, 3370 (1998).
[47] M. P. Faifman, L. I. Men'shikov, L. I. Ponomarev, I. V. Puzynin, T. P. Puzynina, and T. A. Strizh, Z. Phys. D: At., Mol. Clusters **2**, 79 (1986).
[48] A. Scrinzi, K. Szalewicz, and H. J. Monkhorst, Phys. Rev. A **37**, 2270 (1988).
[49] Z. Bačić, J. D. Kress, G. A. Parker, and R. T Pack, J. Chem. Phys. **92**, 2344 (1990).
[50] G. A. Parker and R. T Pack, J. Chem. Phys. **98**, 6883 (1993).
[51] R. T Pack, E. A. Butcher, and G. A. Parker, J. Chem. Phys. **102**, 5998 (1995).
[52] M. R. Harston, I. Shimamura, and M. Kamimura, Phys. Rev. A **45**, 94 (1992).
[53] M. R. Harston, I. Shimamura, and M. Kamimura, Z. Phys. D: At., Mol. Clusters **22**, 635 (1992).
[54] B. R. Johnson, J. Chem. Phys. **67**, 4086 (1977); **69**, 4678 (1978).
[55] M. C. Struensee, G. M. Hale, R. T Pack, and J. S. Cohen, Phys. Rev. A **37**, 340 (1988).
[56] N. F. Mott and H. S. W. Massey, *The Theory of Atomic Collisions*, 3rd ed. (Oxford University Press, Oxford, 1965), p. 404ff.
[57] D. W. Schwenke, Comput. Phys. Commun. **62**, 1 (1991).